Localization of Lindbladian fermions

Foster Thompson [1], Yi Huang [1,2] and Alex Kamenev [1,3]
[1] *School of Physics and Astronomy, University of Minnesota Twin Cities, Minneapolis, Minnesota 55455, USA*
[2] *Condensed Matter Theory Center and Joint Quantum Institute, Department of Physics, University of Maryland, College Park, Maryland 20742, USA*
[3] *William I. Fine Theoretical Physics Institute, University of Minnesota Twin Cities, Minneapolis, Minnesota 55414, USA*

(Received 3 February 2024; revised 23 March 2024; accepted 30 March 2024; published 3 May 2024)

We study a Lindbladian generalization of the Anderson model of localization that describes disordered free fermions coupled to a disordered environment. From finite-size scaling of both eigenvalue statistics and the participation ratio, we identify localization transitions in both the non-Hermitian Lindbladian spectrum, which governs transient relaxation dynamics, and the Hermitian stationary state density matrix. These localization transitions occur at different critical values of the Hamiltonian and dissipative disorder strength, implying the existence of unconventional phases with a mixture of localized and delocalized features. We find that this phenomenon is robust to changes in the value of the dissipative spectral gap.

DOI: 10.1103/PhysRevB.109.174201

I. INTRODUCTION

Disorder-driven phenomena are a central theme in condensed matter physics, with one of the most famous examples being the Anderson model of localization [1–3]. As a successful phenomenological theory of metals and semiconductors, the Anderson model has demonstrated deep connections between generic disordered quantum systems and random matrix theory [4].

In the last few decades, localization in non-Hermitian systems has been extensively studied across various fields of physics, ranging from random lasers to biological networks and many others [5–32]. The earliest and perhaps most well-known instantiation of this phenomenon is the Hatano-Nelson model [5,6,33,34], which describes a dirty one-dimensional metal subject to nonreciprocity between opposite hopping directions. An adequately substantial biased hopping ultimately results in the delocalization of electrons even in one dimension. Another notable example, which partially motivates this work, is a non-Hermitian generalization of the Anderson model with complex-valued local potentials [18,26]. Originally developed to model optical lattices with random gain and loss in the context of disordered photonics and random lasers [12,17–19], this model undergoes a non-Hermitian generalization of Anderson localization in sufficiently high dimension [27–29,35].

One setting exhibiting non-Hermitian physics that has garnered much recent attention is the dynamics of open quantum systems. Under the Markovian approximation, the density matrix of an open quantum system undergoes a non-Hermitian time evolution described by the Lindblad master equation [36,37]. Many existing models of non-Hermitian disorder are unsuitable for modeling open quantum systems because they do not explicitly incorporate incoherent processes coming from interactions with the environment, which inevitably drive the system to a nonequilibrium mixed state at long times. As such, while much of the wisdom obtained from the study of non-Hermitian matrices can be imported to help us understand disordered Lindbladians, there is additional structure present in the Lindbladian setting that past studies do not fully capture, namely, the form of the stationary density matrix.

The interest in studying disorder effects on dissipative open quantum systems is largely attributed to the availability of precisely controlled experiments that can be conducted on specific atomic, molecular, and optical systems. An example of an open quantum system with dissipation involves cold atoms confined within an optical lattice created by counter-propagating lasers, alongside the presence of an additional reservoir of cold atoms [38–41]. These systems feature both gain and loss represented by atoms falling from the reservoir to the lattice and by the escape of atoms from the lattice trap, respectively. Such experiments open up the possibility of discovering unexplored disorder-driven quantum phenomena.

There have been numerous recent theoretical explorations of the effects of disorder in Lindbladian dynamics. Recent attention has been directed toward random matrix models [42–46], demonstrating the connection between generic Lindbladian spectra and non-Hermitian random matrix theory. This association has been suggested as a key feature of dissipative quantum chaos [30,47–49]. Non-Hermitian many-body localization transitions of the Lindbladian spectrum have also recently become an area of active research [50–52].

In addition to the non-Hermitian Lindbladian spectrum, several works have examined the possibility of a nontrivial disorder-induced stationary state. In [53,54], quadratic Lindbladian fermions with all-to-all random matrix couplings were shown to undergo simultaneous transitions in both the spectrum and stationary state as a function of the number of decay channels. Another set of examples is Refs. [55–57], which studied different types of localization transitions in the stationary states of disordered lattice fermions.

In this work, we propose a Lindbladian generalization of the Anderson model which may act as a paradigmatic example

of localization in open quantum systems. This is achieved by introducing processes by which the system can gain and lose particles from and to a disordered environment. To bridge the gap between existing theory on non-Hermitian Anderson transitions and disordered Lindbladians, we construct the model so that it has a spectrum determined by a non-Hermitian Anderson model and also possesses a nontrivial stationary state. This enables us to study the relationship between the localization transitions in the spectrum and the stationary state, which has not previously been examined. We study localization in our model using standard numerical techniques based on finite-size scaling of both Hermitian and non-Hermitian random matrix level statistics and the participation ratio (PR). We find that both the spectrum and the stationary state localize and, strikingly, that these transitions occur at different disorder strengths. This suggests the presence of two intermediate phases between strong and weak disorder, where either the stationary state or transient modes are localized while the other remains spatially extended.

II. MODEL AND RESULTS

Consider a gas of fermions on a three-dimensional square lattice with a total of L^3 sites. Its many-body density matrix ρ obeys the Lindblad equation:

$$\partial_t \rho = -i[\hat{\mathcal{H}}, \rho] + \sum_v \left(\hat{\mathcal{L}}_v \rho \hat{\mathcal{L}}_v^\dagger - \frac{1}{2}\{\hat{\mathcal{L}}_v^\dagger \hat{\mathcal{L}}_v, \rho\} \right). \quad (1)$$

The Hamiltonian is taken to be that of the standard Anderson model,

$$\hat{\mathcal{H}} = \sum_{\mathbf{r}} \varepsilon_{\mathbf{r}} \hat{c}_{\mathbf{r}}^\dagger \hat{c}_{\mathbf{r}} + \sum_{\langle \mathbf{r},\mathbf{r}' \rangle} \hat{c}_{\mathbf{r}}^\dagger \hat{c}_{\mathbf{r}'}, \quad (2)$$

where $\mathbf{r}$ is a lattice vector and $\langle \mathbf{r}, \mathbf{r}' \rangle$ denotes nearest-neighbor sites. The on-site potential $\varepsilon_{\mathbf{r}}$ is random and independently distributed on each site, taken from a box distribution with width W_{R}, $\varepsilon_{\mathbf{r}} \in [-W_{\mathrm{R}}/2, W_{\mathrm{R}}/2]$.

To model coupling to a disordered environment, we allow each site to gain and lose particles at different independent random rates. Each site may be thought of as coupled to two different baths; one pumps particles into the system, and the other acts as a sink to which particles can escape. This is described by two sets of jump operators corresponding to these loss and gain processes, respectively:

$$\hat{\mathcal{L}}_{\mathbf{r}}^{(\mathrm{l})} = \mu_{\mathbf{r}} \hat{c}_{\mathbf{r}}, \quad \hat{\mathcal{L}}_{\mathbf{r}}^{(\mathrm{g})} = \nu_{\mathbf{r}} \hat{c}_{\mathbf{r}}^\dagger. \quad (3)$$

The dissipative couplings $\mu_{\mathbf{r}}$ and $\nu_{\mathbf{r}}$ are taken as random and independently distributed on each site. This choice leads to both nontrivial transient relaxation dynamics and a nontrivial stationary state. The distribution of the dissipative couplings is chosen so that their squares are independently sampled from a box distribution, $\mu_{\mathbf{r}}^2, \nu_{\mathbf{r}}^2 \in [0, W_{\mathrm{I}}]$. The choice of a box distribution simplifies numerical computation and is not expected to modify universal features of the transitions. We note that one could alternatively choose a finite value for the left edge of the distribution, which would put a lower bound on the rate of dissipation of each site. We observe that such a choice does not significantly modify the transitions; see Sec. III C for a detailed discussion of this point.

A. Background

Following the theory of quadratic Lindbladians based on either third quantization [58] or Keldysh techniques [54,59,60], one may introduce three single-particle matrices,

$$(H_0)_{\mathbf{r}\mathbf{r}'} = \varepsilon_{\mathbf{r}} \delta_{\mathbf{r}\mathbf{r}'} + \delta_{\langle \mathbf{r},\mathbf{r}' \rangle}, \quad (4a)$$

$$Q_{\mathbf{r}\mathbf{r}'} = \tfrac{1}{2}\left(\mu_{\mathbf{r}}^2 + \nu_{\mathbf{r}}^2\right)\delta_{\mathbf{r}\mathbf{r}'}, \quad (4b)$$

$$D_{\mathbf{r}\mathbf{r}'} = \left(\mu_{\mathbf{r}}^2 - \nu_{\mathbf{r}}^2\right)\delta_{\mathbf{r}\mathbf{r}'}. \quad (4c)$$

The single-particle eigenvalues of the Lindbladian are equivalent to the eigenvalues of the non-Hermitian dynamic matrix $H = H_0 - iQ$. The corresponding eigenvectors are the single-particle transient modes of the many-body dynamics, governing relaxation to the stationary state.

In contrast, the (unique) stationary state density matrix ρ_{st} is a Gaussian state that can be expressed using an effective Hermitian Hamiltonian,

$$\rho_{\mathrm{st}} \propto \exp\left\{ -\sum_{\mathbf{r},\mathbf{r}'} \hat{c}_{\mathbf{r}}^\dagger \, (H_{\mathrm{st}})_{\mathbf{r}\mathbf{r}'} \, \hat{c}_{\mathbf{r}'} \right\}. \quad (5)$$

The matrix H_{st} may be determined from the stationary Keldysh distribution function F_{st}, which in turn solves a matrix Lyapunov equation [54],

$$F_{\mathrm{st}} = \tanh(H_{\mathrm{st}}/2), \quad (6a)$$

$$i(HF_{\mathrm{st}} - F_{\mathrm{st}}H^\dagger) = D. \quad (6b)$$

The stationary state ρ_{st} is a statistical superposition of free fermion states with different occupation probabilities. The eigenvectors of H_{st} determine the single-particle states, and the eigenvalues specify their corresponding stationary occupation numbers. The uniqueness of the stationary state is a consequence of the absence of conserved quantities in the model. One cannot specify a temperature or chemical potential because neither the energy nor the particle number is conserved.

Thus, two distinct objects, the dynamic matrix H and the stationary Hamiltonian H_{st}, are needed to fully characterize the theory. This should be contrasted with coherent models of disordered free fermions, for which all features of the model can be deduced from the properties of the single-particle Hamiltonian alone once one specifies the temperature and chemical potential.

In the context of the model considered here this presents two distinct random matrix problems, one non-Hermitian and one Hermitian. The dynamic matrix H is similar to a non-Hermitian Anderson model, for example, in Refs. [18,26], but the sampling of the imaginary on-site terms is chosen to ensure the spectrum is supported only below the real axis. This difference can be expected to manifest only in nonuniversal features of the model, so one should anticipate a non-Hermitian Anderson transition in the AI† symmetry class [61,62].

In contrast, the stationary Hamiltonian is specified indirectly through the constraint imposed by the Lyapunov equation (6b). This specifies an unusual random matrix problem which to our knowledge has not been previously studied. The entries of the matrix H_{st} may be complex, placing it in the

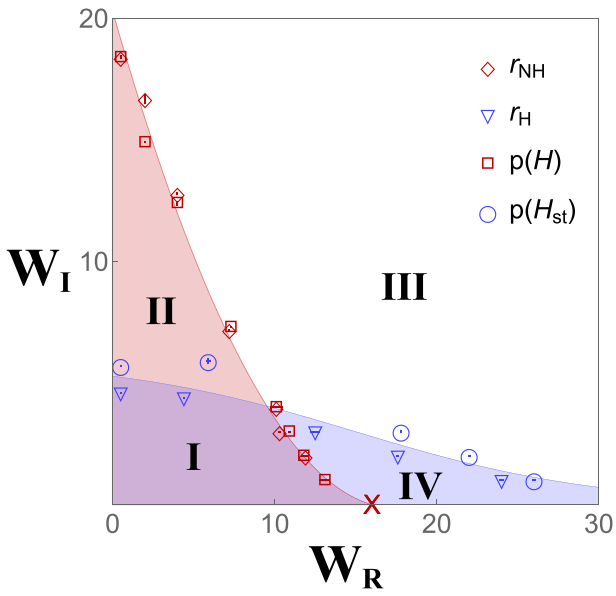

FIG. 1. Effective phase diagram of the three-dimensional model. Dark red and light blue markers denote numerically determined critical disorder strengths (W_R^*, W_I^*) (see Sec. III) for the dynamic matrix H and the stationary state H_{st}, respectively; lines through their centers denote numerical uncertainties. The triangles and diamonds denote values determined from ratio statistics, and circles and squares denote values from the participation ratio. The dark red X on the horizontal axis denotes the critical point of the Hermitian Anderson model. Solid lines illustrate schematic phase boundaries consistent with our numerical estimates which separate four phases, labeled with roman numerals. Phases I and II have delocalized H and delocalized and localized H_{st}, respectively; phases III and IV have localized H and localized and delocalized H_{st}, respectively.

unitary symmetry class A. This is true in spite of the fact that all three single-particle matrices, H_0, Q, and D, have purely real entries. This is a consequence of the dynamic lack of time reversal symmetry: the Lindbladian dynamics describes the irreversible process of a system relaxing to a unique stationary state while in contact with its environment. One may thus expect a localization transition within the unitary universality class.

B. Summary of the main results

The model has two parameters, W_R and W_I, the Hamiltonian and dissipative disorder strengths, respectively. The limit of strong disorder of either type causes both the dynamic matrix H and the stationary state effective Hamiltonian H_{st} to localize. These transitions occur at different critical disorder strengths, resulting in four distinct phases (see Fig. 1). Two phases have a mixture of localized and delocalized features: the stationary state is a statistical mixture of either delocalized or localized states, while the relaxation to this state occurs through the excitation of localized or delocalized transient modes. This phenomenon has no analog in equilibrium, where the state and dynamics are canonically specified by the same Hamiltonian. It is possible in the present context because fluctuations in the stationary state and relaxation dynamics have no fixed relation (no fluctuation-dissipation theorem) in the far-from-equilibrium dynamics studied here.

We further find that the existence of these phases is not strongly contingent on the dissipative spectral gap, the smallest imaginary part of all nonzero Lindbladian eigenvalues. It is, instead, the property of the spectrum near the center of the support of the single-particle matrices, where their density of states is large, that governs the transition, similar to the conventional Hermitian Anderson localization. This suggests that these localization phenomena are conceptually unrelated to the rate of approach to the stationary state and may occur in systems with or without a finite dissipative gap. For a more detailed discussion and justification, see Sec. III C.

We note several additional features of the phase diagram before discussing the details of the transition in Sec. III. The location of the critical line of H is relatively symmetric with respect to W_R vs W_I. This is expected, as similar results hold for the non-Hermitian Anderson model with different real and imaginary disorder strengths [28]. The slight asymmetry in our model comes from the difference in the sampling of real and imaginary on-site potentials. Qualitatively, both play a similar role in driving the localization transition of H. The dissipationless limit $W_I \to 0$ corresponds to $H \to H_0$. The critical line for H intersects the horizontal axis at $W_R \simeq 16$, the known value for Hermitian Anderson localization on a $d = 3$ square lattice with nearest-neighbor hopping [63].

In contrast, the critical line of H_{st} is comparatively quite flat in the horizontal direction. The location of the critical point depends only very weakly on W_R until its value becomes very large. This lack of sensitivity to the Hamiltonian disorder strength suggests that stationary state localization is driven almost exclusively by competition between the coherent hopping and incoherent gain and loss processes. For large W_R, the phase boundary tends toward the horizontal axis. In the range of small W_I and large W_R, denoted phase IV in Fig. 1, H_{st} is delocalized, despite the single-particle Hamiltonian H_0 being strongly localized. The ultimate fate of phase IV for very large W_R is difficult to resolve numerically. It is unclear whether it eventually terminates in a second critical point on the horizontal axis or the stationary state remains delocalized for any large, but finite, W_R. The Lyapunov equation becomes ill defined in the dissipationless limit $W_I = 0$, reducing to a commutator with H_0 and thus lacking a unique solution. The different phases for H_{st} are meaningful only for a finite $W_I > 0$.

III. NUMERICS

We perform a finite-size scaling analysis based on both eigenvalue level statistics and PR on both H and H_{st}. We also examine the localization profile of individual eigenvectors of both through the PR and estimate critical exponents of the transitions. We conclude with a discussion of the role of the dissipative gap.

A. Transient modes

Localization of the dynamic matrix H can be detected through non-Hermitian eigenvalue statistics: letting $s_{1,2}(\epsilon)$ denote the geometric distance in the complex plane between

an H eigenvalue ϵ and its nearest and next-nearest neighbors, respectively, the non-Hermitian level spacing ratio is defined as [30]

$$r_{\rm NH}(W_{\rm R}, W_{\rm I}) = \langle s_1(\epsilon)/s_2(\epsilon)\rangle, \tag{7}$$

where $\langle\cdots\rangle$ is both a disorder average and a sum over all ϵ in a finite-size window centered in the middle of the spectrum of H, the point $(0, -W_{\rm I}/2)$ in the complex plane. The window is defined using a modification of the approach used in [27] as the middle quarter of eigenvalues sorted by the magnitudes of both their real and imaginary parts in terms of how close they are to this point. This quantity has the limiting values $r_{\rm NH} \simeq 0.67$ for uncorrelated eigenvalues in a localized system and $r_{\rm NH} \simeq 0.72$ for symmetry class AI† in a delocalized system [30].

By fixing one of $W_{\rm R,I}$ and varying the other or by imposing a constraint between the two, the curves of $r_{\rm NH}(W)$ for different system sizes L all intersect at a critical point $(W_{\rm I}, W_{\rm R}) = (W_{\rm I}^*, W_{\rm R}^*)$; for an example see Fig. 2. The precise location of the critical point is extracted by fitting data to the scaling form in the vicinity of the transitions,

$$r_{\rm NH}(W) \simeq r_{\rm NH}^* - r_{\rm NH}^{(1)} L^{1/\nu}(W - W^*), \tag{8}$$

where $r_{\rm NH}^*$ is the value of $r_{\rm NH}$ at the critical point, $r_{\rm NH}^{(1)}$ is a constant of proportionality, and ν is the critical exponent of the correlation length.

We verify the existence of the transition by studying the spatial profile of the eigenvectors of H. Using the right eigenvectors of H, given by $H|\epsilon\rangle = \epsilon|\epsilon\rangle$, one may define the participation ratio similarly to that in Hermitian models [64,65]:

$$\mathrm{PR}(\epsilon) = \left[\sum_{\mathbf{r}} \frac{|\langle \mathbf{r}|\epsilon\rangle|^4}{|\langle\epsilon|\epsilon\rangle|^2}\right]^{-1}, \tag{9}$$

where $|\mathbf{r}\rangle$ is the spatial basis on the lattice. Focusing only on the right eigenvectors of H is justified because $H = H^{\rm T}$ and therefore the left eigenvectors are the complex conjugates of the right ones and thus have the same PR. To perform the scaling analysis, we introduce the following quantity:

$$p(W_{\rm R}, W_{\rm I}) = \left\langle \frac{\ln(\mathrm{PR})}{\ln(L^d)} \right\rangle, \tag{10}$$

where $\langle\cdots\rangle$ is the same disorder plus spectral average as used in $r_{\rm NH}$ described above. Near the transition this quantity has the scaling form [66–68]

$$p(W) \simeq p^* - p^{(1)} \frac{L^{1/\nu}}{\ln(L)}(W - W^*), \tag{11}$$

where as in Eq. (8) W is either of $W_{\rm R,I}$ and ν is the critical exponent; p^* is the value of p at the critical point, and $p^{(1)}$ is a constant of proportionality. Examples of the finite-size scaling of both the ratio statistics and the PR are shown in Fig. 2.

This fitting also enables estimation of the critical exponent ν (see Fig. 3). The values found using the ratio statistics are most closely consistent with $\nu \simeq 1.5$ obtained for $d = 3$ in Ref. [27]. The values obtained from the PR are close to $\nu \simeq 1.2$, which, interestingly, is closer to the estimate of $\nu \simeq 1.19$ found in Ref. [28]. This systematic discrepancy is likely attributable to differences in finite-size effects in the PR vs ratio statistics, to which the PR tends to be more sensitive; thus, the ratio statistics should be taken as a more reliable estimate in our analysis. The PR result could be improved by the inclusion of subleading corrections to the scaling ansatz of p, as in, for example, [69]. The present analysis is sufficient to demonstrate the existence of the localization transition, so we leave a more refined analysis of the critical scaling to future work.

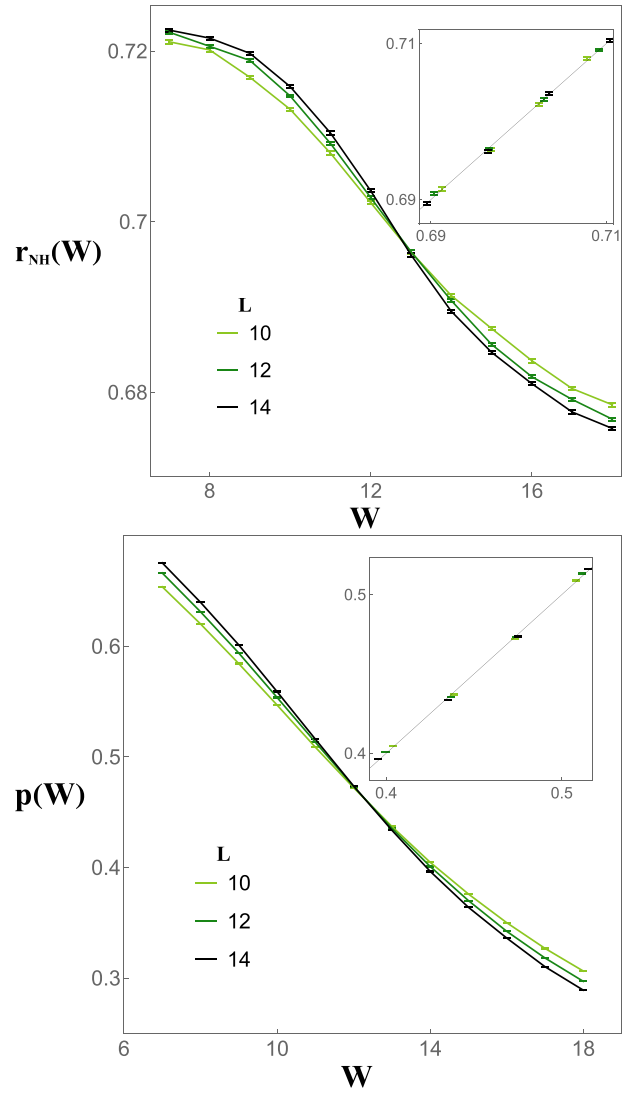

FIG. 2. Examples of finite-size scaling of the level statistics and PR for H, with fixed $W_{\rm R} = 4$. The horizontal axis W on both plots is $W_{\rm I}$; the vertical axes show $r_{\rm NH}$ and p with uncertainties. The crossing points are $W_{\rm I} = 12.77 \pm 0.02$ and 12.36 ± 0.06, respectively, giving critical points in the $(W_{\rm R}, W_{\rm I})$ plane of (4,12.77) and (4,12.36). The insets show computed values of $r_{\rm NH}(W)$ and $p(W)$ using the scaling forms given in Eqs. (8) and (11) with parameters determined from fitting vs their numerically determined values; a solid line with unit slope is shown for reference. The estimated critical exponent is $\nu = 1.44 \pm 0.03$ from level statistics and $\nu = 1.23 \pm 0.02$ from the PR.

We also examine the PR of each eigenvector compared to its location in the complex plane, as shown in Fig. 4. The result is similar to what was observed in Ref. [26]. For a

	(W_R^*, W_I^*)	ν		(W_R^*, W_I^*)	ν
	(11.91±0.12, 2)	1.48±0.19			
	(10.30±0.04, 3)	1.37±0.07		(23.97±0.10, 1)	1.58±0.16
	(10.11±0.35, 4)	1.50±0.61		(17.55±0.04, 2)	1.56±0.08
r_{NH}	(7.19±0.00, 7.19±0.00)	1.50±0.03	r_H	(12.51±0.25, 3)	1.66±0.07
	(0.5, 18.45±0.03)	1.54±0.07		(4.43±0.01, 4.43±0.01)	1.74±0.22
	(2, 16.66±0.16)	1.79±0.21		(0.5, 4.55±0.01)	1.32±0.05
	(4, 12.77±0.02)	1.44±0.03			
	(13.12±0.29, 1)	1.28±0.08			
	(11.84±0.09, 2)	1.22±0.05		(26.05±0.07, 1)	1.44±0.04
	(10.87±0.04, 3)	1.35±0.04		(22.01±0.04, 2)	1.43±0.03
$p(H)$	(10.01±0.08, 4)	1.22±0.05	$p(H_{st})$	(17.77±0.03, 3)	1.54±0.02
	(7.26±0.00, 7.26±0.00)	1.31±0.02		(5.87±0.09, 5.87±0.09)	1.87±0.23
	(0.5, 18.37±0.06)	1.12±0.12		(0.5, 5.72±0.01)	1.45±0.04
	(2, 14.92±0.01)	1.12±0.01			
	(4, 12.36±0.06)	1.23±0.02			

FIG. 3. Fitted values of the localization length critical exponent ν compared to critical disorder strengths (W_R^*, W_I^*) obtained from finite-size scaling analysis of both the ratio statistics and PR for both H and H_{st}, shown with estimated numerical uncertainty.

localized H, eigenvalues are nearly spread over the entire square-shaped region with width W_R and height W_I, with some concentration near the vertical center due to the choice of sampling. For delocalized H, the majority of eigenvalues are concentrated in the middle of the density of states and are delocalized. However, near the boundary of the support region there is a small number of localized states on all sides. This is the complex-plane analog of the mobility edge in the conventional Anderson model. In the present Lindbladian context, it has an additional significance: the eigenvalues closest to the real axis correspond to modes with the smallest decay rate. Since they fall on the edge of the spectrum, this implies that the longest-living transient modes tend to be localized.

B. Stationary state

The stationary state effective Hamiltonian H_{st} undergoes a localization transition in unitary symmetry class A, which is shown for a fixed value of W_I in Fig. 5. To detect this transition, we again use both the ratio statistics and participation ratio. Let β_n denote the nth eigenvalue of H_{st} ordered from smallest to largest and $s_n = \beta_{n+1} - \beta_n$. The level spacing for Hermitian matrices is [24,70]

$$r_H(W_R, W_I) = \left\langle \min\left\{ \frac{s_n}{s_{n-1}}, \frac{s_{n-1}}{s_n} \right\} \right\rangle, \tag{12}$$

where $\langle \cdots \rangle$ is the disorder average and an average over a fraction of eigenvalues in the center of the spectrum of H_{st}, defined using the middle half of the eigenvalues sorted by magnitude. In the localized phase eigenvalues are uncorrelated, and $r_H \simeq 0.39$; in the delocalized phase correlations match the Ginibre unitary ensemble value of $r_H \simeq 0.60$ [70].

Like in the previous section, we identify a transition by fixing one of either $W_{R,I}$ and performing a finite-size scaling analysis by varying the other. The scaling form of r_H is the same as that of r_{NH} shown in Eq. (8). The existence of the transition is confirmed using the PR, which is defined the same way as in Eq. (10). As with H, we find a critical line of transition values of (W_R^*, W_I^*) which separate localized and

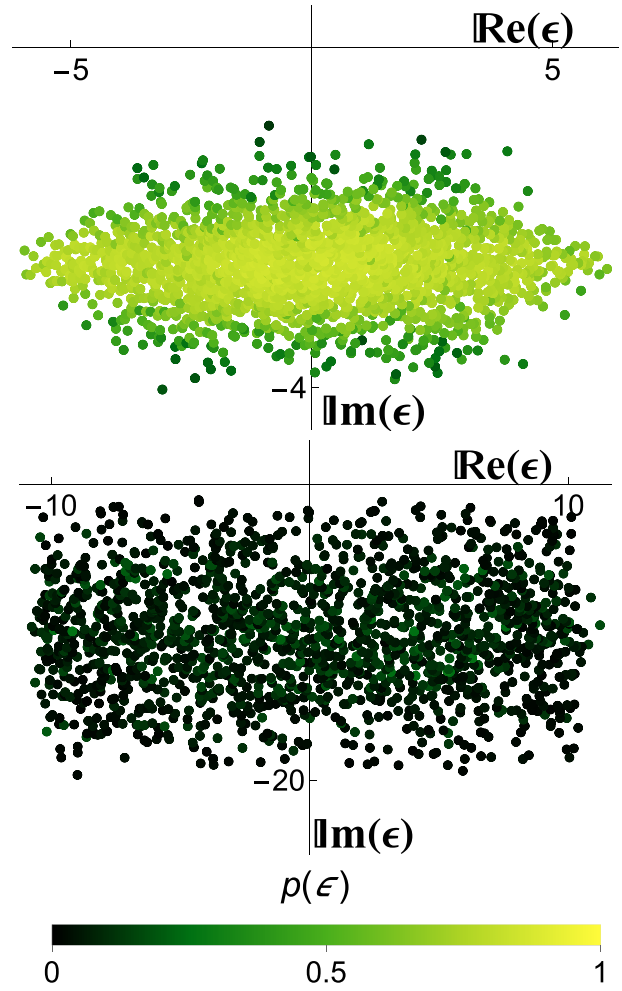

FIG. 4. Complex spectra of H with $L = 12$ and $(W_R, W_I) = (5, 5)$ above and $(W_R, W_I) = (20, 20)$ below. Marker locations show the location of H eigenvalues in the complex plane. Colors indicate the value of $p(\epsilon) = \ln(PR(\epsilon))/\ln(L^3)$, so that the darker the marker color the more localized the corresponding eigenmode is.

delocalized phases of H_{st}, as shown in Fig. 1. The scaling exponent estimates predicted from both ratio statistics are close to known results, for example, in Refs. [71,72], in which the $d = 3$ Anderson transition in symmetry class A was found to have a critical exponent which is close to $\nu \simeq 1.44$ (see Fig. 3). We note that there is a systematic discrepancy in the critical disorder strength predicted by the PR and ratio statistics, which we suggest may be understood similarly to that found in the critical exponents of the non-Hermitian transition (see Sec. III A).

We also observe that the overall shape of the distribution of the PR over the spectrum of H_{st} is substantially more pronounced than that of the corresponding H_0 (see Fig. 6). In the delocalized phase the distribution exhibits a clear mobility edge, much sharper than that of H_0, which shows a prevalence of delocalized states with a large PR at the center of its density of states and states that are more localized with a smaller PR near the edges. This demonstrates the strong sensitivity of the stationary state to the dissipative disorder. We also note that the bandwidth of H_{st} is quite small compared to that of

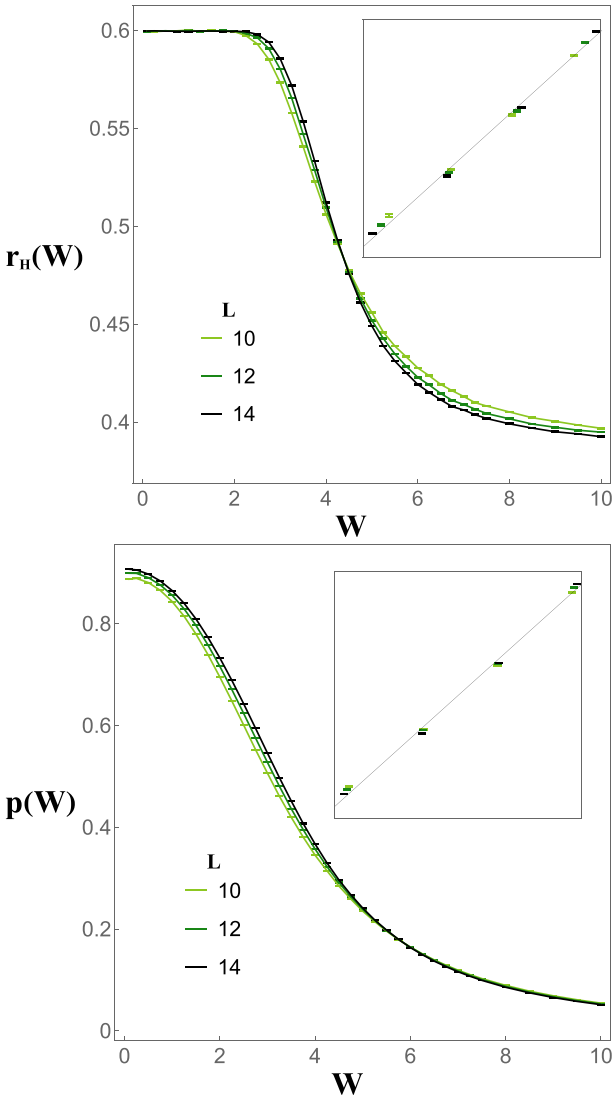

FIG. 5. Examples of finite-size scaling of the level statistics and PR for H_0, with fixed $W_R = W_I$. The horizontal axis shows varying values of $W = W_{R,I}$; the vertical axes show r_H and p with uncertainties. The crossing points are $W = 4.43 \pm 0.01$ and 5.87 ± 0.09, respectively, giving critical points (4.43,4.43) and (5.87,5.87). The insets show computed values of $r_{NH}(W)$ and $p(W)$ using the scaling forms given in Eqs. (8) and (11) with parameters determined from fitting vs their numerically determined values; a solid line with unit slope is shown for reference. The estimated critical exponent is $\nu = 1.74 \pm 0.22$ from level statistics and $\nu = 1.87 \pm 0.24$ from the PR.

H_0, especially in the delocal phase; this can be understood as a consequence of the fact that loss and gain processes have equal strength on average and thus drive the system close to a Gibbs state.

These numerical findings also justify our focus on the eigenstates of H_{st} near the center of its density of states to identify the transition. For delocalized stationary states the bandwidth of H_{st} is small, implying that all eigenstates contribute to expectation values with roughly equal probability. The density of states near the middle is much larger than the edge, so observables are dominated by delocalized features. In

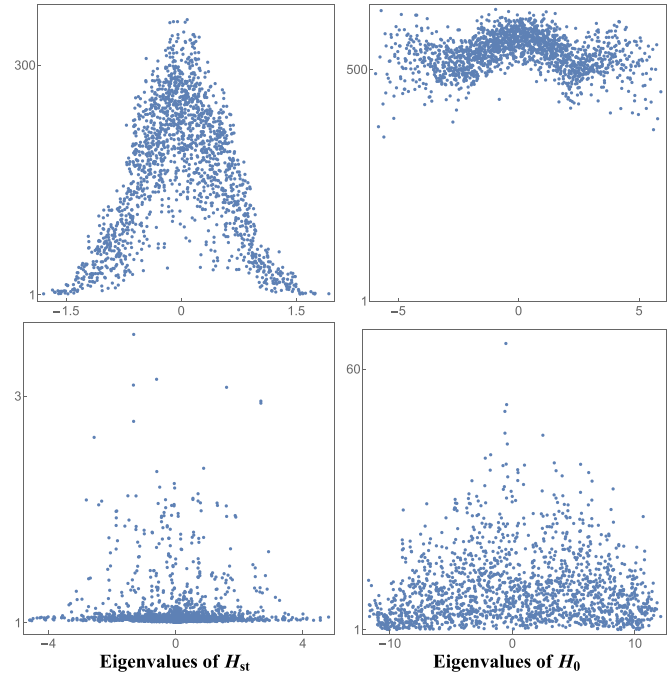

FIG. 6. Participation ratios (vertical axes on all plots) for the eigenvectors of the steady-state effective Hamiltonian H_{st} (left column) and the corresponding Anderson Hamiltonian H_0 (right column) from the same disorder realization, shown for $L = 12$. The bottom row shows $(W_R, W_I) = (20, 20)$, where both plots are in the delocal phase; the top row shows $(W_R, W_I) = (2, 2)$, where both plots are localized.

contrast, for localized stationary states all states are localized, so expectation values always show localized features.

C. Dissipative gap

The dissipative gap determines the slowest rate of approach toward the stationary state from an arbitrary initial state. Formally, it is the minimum of the imaginary part of the Lindbladian spectrum. Systems with a finite dissipative gap decay toward the stationary state exponentially with the timescale given by the inverse gap. Systems without a gap, in contrast, can decay algebraically.

For the quadratic Lindbladian dynamics considered here, the many-body dissipative gap is the same as that of H. Any particular disorder realization exhibits a finite dissipative gap (although this may be lost in the limit $L \to \infty$). In particular, when H is strongly localized, the eigenvalues of H are determined almost exactly by local $\varepsilon_{\mathbf{r}}$, $\mu_{\mathbf{r}}$, and $\nu_{\mathbf{r}}$ and thus fill the entire square-shaped region in the complex plane bound by the real and imaginary intervals $[-W_R/2, W_R/2]$ and $[0, W_I]$. Because both $\mu_{\mathbf{r}}$ and $\nu_{\mathbf{r}}$ can be arbitrarily small, eigenvalues can be arbitrarily close to the real axis, leading to a vanishing dissipative gap.

While this is true of the model as defined above, we argue that this is not an essential feature of either type of localization observed here. Modification of the jump operators can introduce a finite dissipative gap even in the strongly localized regime of either or both of H and H_{st}. To show this, we consider an additional set of nonrandom gain and loss channels

encoded by two additional sets of jump operators:

$$\hat{\mathcal{L}}_{\mathbf{r}}^{(\mathrm{I}')} = \sqrt{\kappa}\,\hat{c}_{\mathbf{r}}, \quad \hat{\mathcal{L}}_{\mathbf{r}}^{(\mathrm{g}')} = \sqrt{\kappa}\,\hat{c}_{\mathbf{r}}^{\dagger}, \tag{13}$$

where κ is a site-independent constant. This addition modifies the single-particle matrix Q of Eq. (4),

$$Q_{\mathbf{r}\mathbf{r}'} = \tfrac{1}{2}\left(\mu_{\mathbf{r}}^2 + \nu_{\mathbf{r}}^2 + 2\kappa\right)\delta_{\mathbf{r}\mathbf{r}'}. \tag{14a}$$

The other two single-particle matrices are unchanged. Note that the same result could have been achieved by modifying the distribution of $\mu_{\mathbf{r}}$ and $\nu_{\mathbf{r}}$ so that their squares are uniformly distributed on the shifted interval $[\kappa, W_{\mathrm{I}} + \kappa]$ instead of introducing new jump operators.

This translates the entire spectrum of H away from the real axis by a distance κ in the complex plane, so the dissipative gap is at least as large as κ regardless of the strength of the disorder. This change does not modify any other details of the eigenvalues or eigenvectors. The non-Hermitian Anderson transition is thus unaffected, and the critical line for H in the $(W_{\mathrm{R}}, W_{\mathrm{I}})$ plane, depicted in Fig. 1, is unchanged. The effects on the stationary state are less obvious, but we numerically verified that its localization transition remains intact and the locations of the critical points are not affected for small, but finite, κ. We find that the locations of critical points generally move toward the origin of $(W_{\mathrm{R}}, W_{\mathrm{I}})$ with increasing κ but remain finite (see Fig. 7).

IV. CONCLUSION

We proposed a simple Lindbladian model of localization in an open system of disordered fermions. By studying both eigenvalue statistics and the participation ratio, we found that both the transient modes and the stationary state undergo localization transitions at sufficiently strong disorder of either the Hamiltonian or dissipative type. We established a schematic phase diagram of our model and estimated the localization length critical exponent of the two transitions, which generally agreed with known results for their respective universality classes along the entire phase boundary.

Surprisingly, we found that the stationary state is much more sensitive to the dissipative disorder, while the transient mode spectrum is affected by both types of disorder in an approximately symmetric way. As a consequence, localizations of the transient modes and stationary state occur at different critical disorder strengths. This results in four distinct phases: two conventional phases corresponding to weak and strong disorder of both types in which all features are delocalized or localized, respectively, and two unconventional phases in which only the stationary state or transient modes are localized while the other remains delocalized. We showed that the phases persist independently of the presence of a dissipative spectral gap.

One may speculate on the observable consequences of these new types of localization. Following Ref. [54], expectation values of observables and their equal-time higher correlation functions depend only on H_{st}. The dynamic matrix H determines observables' nonstationary properties, such as linear response features and quenches from initially nonstationary states. Measurements of local quantities cannot detect a sharp transition between localized and delocalized phases.

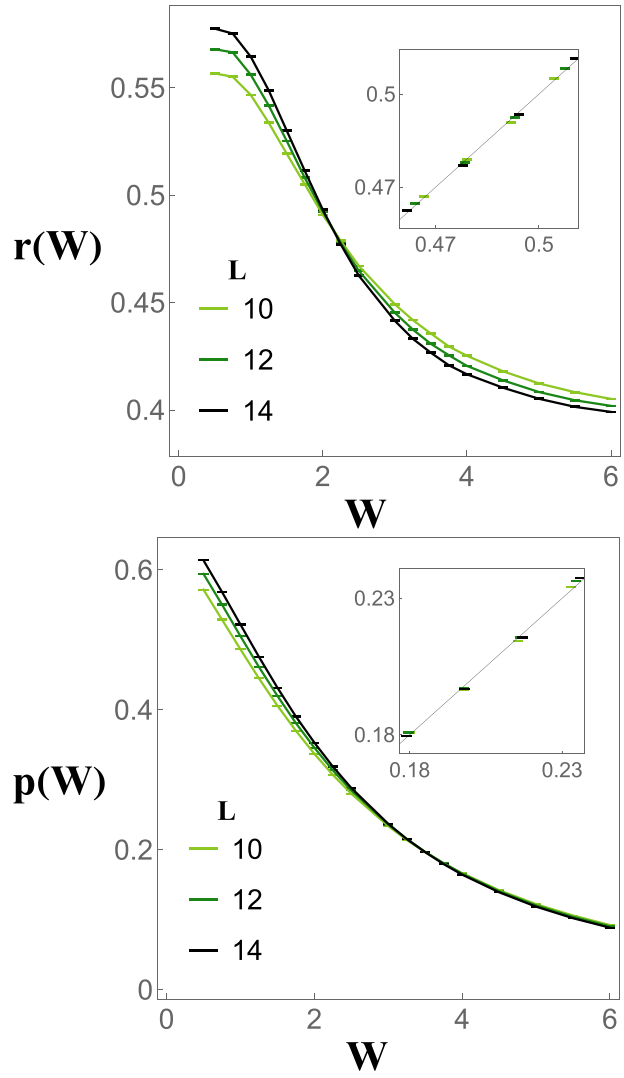

FIG. 7. Finite-size scaling of level statistics and PR for H_{st} with $\kappa = 1$ and $W_{\mathrm{R}} = W_{\mathrm{I}}$ (compare to Fig. 5). The horizontal axis shows varying values of $W = W_{\mathrm{R,I}}$, and the vertical axes show r_{H} and p with uncertainties. The crossing points are $W_{\mathrm{I}} = 3.53 \pm 0.03$ and 2.17 ± 0.002, respectively, giving critical points (3.53,3.53) and (2.17,2.17). The insets show computed values of $r_{\mathrm{H}}(W)$ and $p(W)$ using the scaling forms given in Eqs. (8) and (11) with parameters determined from fitting vs their numerically determined values; a solid line with unit slope is shown for reference. The estimated critical exponent is $\nu = 1.32 \pm 0.05$ from level statistics and $\nu = 1.57 \pm 0.12$ from PR.

In the Hermitian Anderson model, localization is signaled by vanishing conductivity. Such a metric is unsuitable in the model studied here because it has no conserved quantities and hence no transport features. We leave the question of an appropriate experimental signature of localization in this model to future work.

A possible alternative way forward is the construction of a more complicated Lindbladian model with similar localization phenomena that also possesses conserved quantities. In such a theory, transport features could be a signal of localization. This would necessitate going beyond the single-particle description, as the inclusion of conserved quantities

requires jump operators that are at least quadratic in fermion creation operators. It is an open question as to whether or not mixed localized and delocalized features could be realized in disordered many-body Lindbladians. As an alternative to nonlinear jump operators, one may also consider the effects of coherent nonlinearities on the localization of either the transient modes or stationary state. In the three-dimensional model studied here one would anticipate fermion interactions to overcome either type of localization, analogous to closed systems of disordered three-dimensional fermions. The fate of localization in lower dimensions is less obvious. Non-Hermitian versions of many-body localization in one dimension have been studied in the past [25] and recently in the context of Lindbladian spectra in [50–52], but localization features of many-body stationary states have yet to be considered and would be an interesting direction for future study.

ACKNOWLEDGMENTS

We are indebted to B. Shklovskii for stimulating discussions. The work was supported by NSF Grants No. DMR-2037654 and No. DMR-2338819. We acknowledge support from the Simons Foundation Targeted Grant No. 920184 to the Fine Theoretical Physics Institute at the University of Minnesota. Y. Huang was supported by the Laboratory for Physical Sciences.

[1] P. W. Anderson, Phys. Rev. **109**, 1492 (1958).
[2] E. Abrahams, P. W. Anderson, D. C. Licciardello, and T. V. Ramakrishnan, Phys. Rev. Lett. **42**, 673 (1979).
[3] P. W. Anderson, Proc. Natl. Acad. Sci. USA **69**, 1097 (1972).
[4] B. I. Shklovskii, B. Shapiro, B. R. Sears, P. Lambrianides, and H. B. Shore, Phys. Rev. B **47**, 11487 (1993).
[5] N. Hatano and D. R. Nelson, Phys. Rev. Lett. **77**, 570 (1996).
[6] N. Hatano and D. R. Nelson, Phys. Rev. B **58**, 8384 (1998).
[7] D. S. Wiersma, P. Bartolini, A. Lagendijk, and R. Righini, Nature (London) **390**, 671 (1997).
[8] H. Cao, Y. G. Zhao, S. T. Ho, E. W. Seelig, Q. H. Wang, and R. P. H. Chang, Phys. Rev. Lett. **82**, 2278 (1999).
[9] C. Vanneste and P. Sebbah, Phys. Rev. Lett. **87**, 183903 (2001).
[10] D. N. Christodoulides, F. Lederer, and Y. Silberberg, Nature (London) **424**, 817 (2003).
[11] M. Störzer, P. Gross, C. M. Aegerter, and G. Maret, Phys. Rev. Lett. **96**, 063904 (2006).
[12] D. S. Wiersma, Nat. Phys. **4**, 359 (2008).
[13] T. Schwartz, G. Bartal, S. Fishman, and M. Segev, Nature (London) **446**, 52 (2007).
[14] J. Topolancik, B. Ilic, and F. Vollmer, Phys. Rev. Lett. **99**, 253901 (2007).
[15] Y. Lahini, A. Avidan, F. Pozzi, M. Sorel, R. Morandotti, D. N. Christodoulides, and Y. Silberberg, Phys. Rev. Lett. **100**, 013906 (2008).
[16] T. Sperling, W. Bührer, C. M. Aegerter, and G. Maret, Nat. Photon. **7**, 48 (2013).
[17] D. S. Wiersma, Nat. Photon. **7**, 188 (2013).
[18] A. Basiri, Y. Bromberg, A. Yamilov, H. Cao, and T. Kottos, Phys. Rev. A **90**, 043815 (2014).
[19] S. Schönhuber, M. Brandstetter, T. Hisch, C. Deutsch, M. Krall, H. Detz, A. M. Andrews, G. Strasser, S. Rotter, and K. Unterrainer, Optica **3**, 1035 (2016).
[20] D. R. Nelson and N. M. Shnerb, Phys. Rev. E **58**, 1383 (1998).
[21] K. Rajan and L. F. Abbott, Phys. Rev. Lett. **97**, 188104 (2006).
[22] A. Amir, N. Hatano, and D. R. Nelson, Phys. Rev. E **93**, 042310 (2016).
[23] G. H. Zhang and D. R. Nelson, Phys. Rev. E **100**, 052315 (2019).
[24] V. Oganesyan and D. A. Huse, Phys. Rev. B **75**, 155111 (2007).
[25] R. Hamazaki, K. Kawabata, and M. Ueda, Phys. Rev. Lett. **123**, 090603 (2019).
[26] A. F. Tzortzakakis, K. G. Makris, and E. N. Economou, Phys. Rev. B **101**, 014202 (2020).
[27] Y. Huang and B. I. Shklovskii, Phys. Rev. B **101**, 014204 (2020).
[28] X. Luo, T. Ohtsuki, and R. Shindou, Phys. Rev. B **104**, 104203 (2021).
[29] X. Luo, T. Ohtsuki, and R. Shindou, Phys. Rev. Lett. **126**, 090402 (2021).
[30] L. Sá, P. Ribeiro, and T. Prosen, Phys. Rev. X **10**, 021019 (2020).
[31] G. De Tomasi and I. M. Khaymovich, Phys. Rev. B **106**, 094204 (2022).
[32] G. De Tomasi and I. M. Khaymovich, Phys. Rev. B **108**, L180202 (2023).
[33] K. Kawabata and S. Ryu, Phys. Rev. Lett. **126**, 166801 (2021).
[34] N. Hatano and H. Obuse, Ann. Phys. (NY) **435**, 168615 (2021).
[35] Y. Huang and B. I. Shklovskii, Phys. Rev. B **102**, 064212 (2020).
[36] H. Breuer and F. Petruccione, *The Theory of Open Quantum Systems* (Oxford University Press, Oxford, 2002).
[37] C. W. Gardiner and P. Zoller, *Quantum Noise* (Springer, Berlin, 2004).
[38] I. Bloch, Nat. Phys. **1**, 23 (2005).
[39] L. J. LeBlanc and J. H. Thywissen, Phys. Rev. A **75**, 053612 (2007).
[40] I. Bloch, J. Dalibard, and W. Zwerger, Rev. Mod. Phys. **80**, 885 (2008).
[41] M. A. Cazalilla and A. M. Rey, Rep. Prog. Phys. **77**, 124401 (2014).
[42] S. Denisov, T. Laptyeva, W. Tarnowski, D. Chruściński, and K. Życzkowski, Phys. Rev. Lett. **123**, 140403 (2019).
[43] T. Can, J. Phys. A **52**, 485302 (2019).
[44] T. Can, V. Oganesyan, D. Orgad, and S. Gopalakrishnan, Phys. Rev. Lett. **123**, 234103 (2019).
[45] L. Sá, P. Ribeiro, and T. Prosen, J. Phys. A **53**, 305303 (2020).
[46] S. Lange and C. Timm, Chaos **31**, 023101 (2021).
[47] J. Li, T. Prosen, and A. Chan, Phys. Rev. Lett. **127**, 170602 (2021).
[48] A. Kulkarni, T. Numasawa, and S. Ryu, Phys. Rev. B **106**, 075138 (2022).
[49] L. Sá, P. Ribeiro, and T. Prosen, Phys. Rev. Res. **4**, L022068 (2022).

[50] R. Hamazaki, M. Nakagawa, T. Haga, and M. Ueda, arXiv:2206.02984.
[51] F. Roccati, F. Balducci, R. Shir, and A. Chenu, Phys. Rev. B **109**, L140201 (2024).
[52] G. D. Tomasi and I. M. Khaymovich, arXiv:2311.00019.
[53] J. Costa, P. Ribeiro, A. D. Luca, T. Prosen, and L. Sá, SciPost Phys. **15**, 145 (2023).
[54] F. Thompson and A. Kamenev, Ann. Phys. (NY) **455**, 169385 (2023).
[55] A. Beck and M. Goldstein, Phys. Rev. B **103**, L241401 (2021).
[56] A. C. C. de Albornoz, D. C. Rose, and A. Pal, arXiv:2303.07070.
[57] I. Yusipov, T. Laptyeva, S. Denisov, and M. Ivanchenko, Phys. Rev. Lett. **118**, 070402 (2017).
[58] T. Prosen, New J. Phys. **10**, 043026 (2008).
[59] A. Kamenev, *Field Theory of Non-equilibrium Systems* (Cambridge University Press, Cambridge, 2023).
[60] L. M. Sieberer, M. Buchhold, and S. Diehl, Rep. Prog. Phys. **79**, 096001 (2016).
[61] K. Kawabata, K. Shiozaki, M. Ueda, and M. Sato, Phys. Rev. X **9**, 041015 (2019).
[62] R. Hamazaki, K. Kawabata, N. Kura, and M. Ueda, Phys. Rev. Res. **2**, 023286 (2020).
[63] A. MacKinnon and B. Kramer, Phys. Rev. Lett. **47**, 1546 (1981).
[64] R. J. Bell and P. Dean, Discuss. Faraday Soc. **50**, 55 (1970).
[65] R. J. Bell, Rep. Prog. Phys. **35**, 1315 (1972).
[66] A. D. Mirlin and F. Evers, Phys. Rev. B **62**, 7920 (2000).
[67] F. Evers and A. D. Mirlin, Phys. Rev. Lett. **84**, 3690 (2000).
[68] J. Brndiar and P. Markoš, Phys. Rev. B **74**, 153103 (2006).
[69] C. Wang and X. R. Wang, Phys. Rev. B **107**, 024202 (2023).
[70] Y. Y. Atas, E. Bogomolny, O. Giraud, and G. Roux, Phys. Rev. Lett. **110**, 084101 (2013).
[71] K. Slevin and T. Ohtsuki, J. Phys. Soc. Jpn. **85**, 104712 (2016).
[72] T. Wang, T. Ohtsuki, and R. Shindou, Phys. Rev. B **104**, 014206 (2021).